

# The fitness landscape of the codon space across environments

Inês Fragata <sup>\* 1,+</sup>, Sebastian Matuszewski <sup>†2,3,+</sup>, Mark A. Schmitz<sup>1</sup>, Thomas Bataillon<sup>4</sup>,  
Jeffrey D. Jensen<sup>2,3,5</sup>, and Claudia Bank<sup>1</sup>

<sup>1</sup>Instituto Gulbenkian de Ciência, Oeiras, Portugal

<sup>2</sup>School of Life Sciences, Ecole Polytechnique Federale de Lausanne (EPFL), Lausanne  
Switzerland

<sup>3</sup>Swiss Institute of Bioinformatics (SIB), Lausanne, Switzerland

<sup>4</sup>Bioinformatics Research Centre, Aarhus University, 8000, Denmark

<sup>5</sup>School of Life Sciences, Arizona State University, Tempe, USA

<sup>+</sup>These authors contributed equally

## Abstract

Fitness landscapes map the relationship between genotypes and fitness. However, most fitness landscape studies ignore the genetic architecture imposed by the codon table and thereby neglect the potential role of synonymous mutations. To quantify the fitness effects of synonymous mutations, we used a new software based on Bayesian Monte Carlo Markov Chain methods and estimated selection coefficients from deep sequencing data obtained across 9 amino-acid positions from Hsp90 in *Saccharomyces cerevisiae*. This work demonstrates how topology and topography of the codon fitness landscape change when synonymous effects are considered. This impacts how populations traverse fitness space as well as their likelihood of reaching a global optimum, in particular in a stressful environment. Finally, we show that residue position, mRNA stability, and codon frequency are predictors of synonymous effect size. Together these results highlight the role of synonymous mutations in adaptation and demonstrate the potential mis-inference when they are neglected in fitness landscape studies.

---

\*irfragata@gmail.com

†sebastian.matuszewski@hotmail.com



42 position in the genome contains a fitness landscape that consists of the  $(4^{\text{nucleotides}})^{3^{\text{loci}}} = 64$   
43 codons at that position. Whereas from the amino-acid view of the landscape, each transition  
44 is possible in a single step, the codon based landscape requires up to three mutational steps to  
45 transition from one amino-acid to another. This results in a different topology of the fitness  
46 landscape with a reduced connectivity (i.e., fewer neighboring genotypes) and larger mutational  
47 step size between any two amino-acid genotypes (c.f. Fig. 1 A & B). Moreover, a single-nucleotide  
48 mutation in a codon based landscape can result in only 5 to 7 amino-acid changes rather than  
49 the 20 total possible amino-acid changes. Thus, at a single amino-acid position, a codon based  
50 fitness landscape (with 64 genotypes) can be multi-peaked, whereas the corresponding amino-  
51 acid landscape (with 21 genotypes) is by definition single-peaked.

52 Furthermore, mutations in an amino-acid based fitness landscape are, by definition, non-synonymous.  
53 This neglects accumulating evidence from both comparative and experimental studies that syn-  
54 onymous mutations (i.e., mutations that change the codon but not the encoded amino-acid  
55 sequence) can display non-negligible fitness effects (Singh *et al.*, 2007; Drummond and Wilke,  
56 2008; Kudla *et al.*, 2009; Zhou *et al.*, 2009; Lind *et al.*, 2010; Plotkin and Kudla, 2011; Sauna and  
57 Kimchi-Sarfaty, 2011; Agashe *et al.*, 2013; Bailey *et al.*, 2014; Firnberg *et al.*, 2014; Hunt *et al.*,  
58 2014; Bali and Bebok, 2015; Presnyak *et al.*, 2015; Agashe *et al.*, 2016; Choi and Aquadro, 2016;  
59 Knöppel *et al.*, 2016). For example, recent studies have shown that synonymous mutations can  
60 affect the speed and accuracy of translation (Drummond and Wilke, 2008; Saunders and Deane,  
61 2010; Plotkin and Kudla, 2011; Bali and Bebok, 2015), mRNA structure (Shabalina *et al.*, 2013;  
62 O'Brien *et al.*, 2014; Presnyak *et al.*, 2015), expression in response to environmental changes  
63 (Shabalina *et al.*, 2013), and that they are associated with several organismal malfunctions  
64 (Parmley and Hurst, 2007; Hunt *et al.*, 2014). Although synonymous effects undoubtedly exist,  
65 effect sizes are often small, which has made a systematic characterization difficult. In particular,  
66 to our knowledge there exists no study to date that has characterized whether fitness effects of  
67 synonymous mutations vary across environments; a finding that could be in concordance with  
68 the costs of adaptation that are frequently reported for amino-acid changing mutations (e.g.  
69 Bataillon *et al.*, 2011; Wenger *et al.*, 2011; Hietpas *et al.*, 2013; Rodriguez-Verdugo *et al.*, 2014).  
70 Thus, when fitness landscapes are defined on the codon level instead of the amino-acid level  
71 both its topology (i.e., the number and connectivity of genotypes) and its topography (i.e., the  
72 fitness relationship between genotypes; Fig. 1) change. As highlighted by Zagorski *et al.* (2016),  
73 a change in the topology of a fitness landscapes can result in dramatically different conclusions  
74 about the accessibility of fitness peaks, and the topography further amplifies this effect.

75 Here we use published data (Bank *et al.*, 2014) from deep mutational scanning (Fowler and  
76 Fields, 2014) to study the codon based fitness landscapes of the same 9 amino-acid positions  
77 across 6 environments. We first establish that synonymous mutations indeed affect fitness, and  
78 then quantify their associated distribution of fitness effects. To this end, we present *empiricIST*,  
79 a software that allows for accurate estimation of selection coefficients and credibility intervals  
80 from bulk competitions. We then study how considering individual effects of synonymous mu-  
81 tations changes conclusions about both accessibility and ruggedness of the landscapes, and thus  
82 the potential for adaptation. By comparing single-effect landscapes to their corresponding aver-  
83 aged landscapes, which neglect the effects of synonymous mutations (Fig. 1 C & D), we quantify  
84 how synonymous mutations affect the topography of the fitness landscapes while keeping the  
85 topology fixed. Finally, we use regression models to dissect the contribution of environmental  
86 *versus* molecular variables to the observed effects of synonymous mutations. Our work provides  
87 the first characterization of the distribution of fitness effects of synonymous mutations across  
88 environments, and calls for a more careful consideration of synonymous effects in future studies  
89 of fitness landscapes and adaptive walks.

## 90 **2 Material & Methods**

### 91 **2.1 MCMC Method**

92 We provide a software package for 1) processing sequencing count data from deep mutational  
93 scanning (DMS) experiments, 2) estimating growth rates using a Bayesian MCMC approach  
94 described in detail in (Bank *et al.*, 2014), and 3) post-processing of growth rate estimates to  
95 estimate the shape of the beneficial tail of the distribution of fitness effects (DFE). A detailed  
96 description of the software, its usage, and options can be found in the accompanying manual  
97 (<https://github.com/Matu2083/empiricIST>). In the following, we give a brief description of the  
98 assumed experimental setup and the model underlying the MCMC and estimation procedure,  
99 and by means of simulations compare the accuracy of the results to that obtained from conven-  
100 tional linear regression (Matuszewski *et al.*, 2016).

#### 101 *Assumptions of the model and input data*

102 We consider an experiment assessing the fitness of  $K$  mutants, labelled  $i \in \{1, \dots, K\}$ . Each  
103 mutant  $i$  is assumed to be present at initial population size  $c_i$  and to grow exponentially at

104 constant rate  $r_i$ , such that its true abundance at time  $t$ ,  $N_i(t)$ , is given by  $N_i(t) = c_i \exp^{r_i t}$ . At  
105 each sampling time point  $t \in \{1, \dots, T\}$ , sequencing reads  $n_{i,t}$  are drawn from a multinomial  
106 distribution with parameters  $n_t = \sum_{i=1}^K n_{i,t}$  (i.e., the total number of sequencing reads) and  
107  $p_t = (p_{1,t}, \dots, p_{K,t})$ , where  $p_{i,t} = \frac{c_i \exp^{r_i t}}{\sum_{i=1}^K c_i \exp^{r_i t}}$  is the relative frequency of mutant  $i$  in the  
108 population at time  $t$ . Here, time is measured in hours to make results comparable across  
109 different environmental conditions (Chevin, 2011; Bank *et al.*, 2014). The software allows for  
110 input of either generation or standard time. We furthermore assume that sampling points are  
111 independent such that the overall likelihood can be written as the product of the individual  
112 likelihoods of each sampling point.

$$L(n) = \prod_{t \in T} L(c, r | \{n_{1,t}, \dots, n_{K,t}\}).$$

113 All initial population sizes  $c_i$  and growth rates  $r_i$  are estimated relative to those of a chosen  
114 reference mutant with its initial population size and growth rate arbitrarily set to 10 000 and  
115 1, respectively. Here, the wild-type sequence in laboratory conditions of 30°C was used as the  
116 reference.

### 117 *MCMC model*

118 We implemented a Metropolis-Hastings algorithm in C++ using flat priors allowing all attainable  
119 values  $r_i \in R^+$  and  $c_i \in N$  to be realized with equal probability. During the burn-in period the  
120 variance of both proposal distributions was adjusted such that the targeted acceptance ratio is  
121 around 25%, which optimizes the performance the MCMC chain (Gelman *et al.*, 1996).

122 The updated variance of the proposal distribution is calculated using

$$\sigma_{\text{new}} = \sigma_{\text{old}} f(k; y, k)$$

with

$$f(x; y, k) = \left[ 1 + \frac{(\cosh(x - y) - 1)(k - 1)}{\cosh(y - |x - y|) - 1} \right] \text{sgn}(x - y),$$

123 where  $x$  denotes the targeted acceptance ratio,  $y$  is the current acceptance ratio, and  $k$  is a (fixed)  
124 scale parameter that restricts the maximal change in the variance of the proposal distribution.  
125 After discarding the first 100 000 accepted samples (i.e., after the burn-in period), the MCMC

126 was run for an additional 10 000 000 accepted samples. Only every 1000th sample was retained  
 127 for further analyses, such that the posterior distribution of each parameter was characterized by  
 128 10 000 samples overall.

129 Convergence and mixing were checked by visual inspection of the resulting trace files for all  
 130 estimated parameters, and by calculating the effective sample sizes (i.e., the number of inde-  
 131 pendent samples) and the Hellinger distance (Boone *et al.*, 2014) between sets of 1000 batched  
 132 recorded samples. Effective sample sizes were generally larger than 1000 for all parameters, and  
 133 Hellinger distances below 0.1 indicated convergence and good mixing. To facilitate estimation,  
 134 we took advantage of the fact that the multinomial distribution is preserved when a subset of  
 135 the counting variables are observed. This enabled us to split the data set into sub-data sets with  
 136 10 mutants each (implicitly treating the other mutants' sequencing reads as observed). More  
 137 options such as outlier detection, data imputation, DFE tail-shape estimation are detailed in  
 138 the Supporting Information.

### 139 *Assessing accuracy of the MCMC*

140 To assess the accuracy of the Bayesian MCMC approach, we compared its parameter estimates  
 141 to those obtained using ordinary least squares (OLS) linear regression of the log-ratios against  
 142 the number of sequencing reads  $n_{i,t}$  over the different sampling time points (Matuszewski *et al.*,  
 143 2016). For that we simulated time-sampled deep sequencing data (implemented in C++; avail-  
 144 able from <https://github.com/Matu2083/empiricIST>), assuming that individual mutant growth  
 145 rates and initial population sizes for each of the  $K$  mutants are drawn independently from a  
 146 normal distribution (i.e.,  $r_i \sim \mathcal{N}(1, 0.01)$ ) and a log-normal distribution (i.e.,  $c_i \sim 10^{\mathcal{N}(4, 0.25)}$ ),  
 147 respectively. Without loss of generality, we denote the wild-type reference (or any other reference  
 148 genotype) by  $i = 1$  and set its growth rate to 1. Sequencing reads were then drawn independently  
 149 for each of the  $T$  equally spaced time points from a multinomial distribution with parameters  
 150  $n_t$  (i.e., the number of total sequencing reads per time point) and  $p_t = (p_{1,t}, \dots, p_{K,t})$ . To check  
 151 the robustness of these results when applied to the real experimental data, we furthermore drew  
 152 growth rates from a mixture distribution

$$153 \quad r_i \sim \begin{cases} |N(1, \hat{\sigma})| & \text{if } z = 0, \\ \exp(\hat{\lambda}) + 1 & \text{if } z = 1, \end{cases}$$

154 where  $Z \sim \mathcal{B}(x)$  is a Bernoulli-distributed random variable that indicates whether growth rates  
 155 are drawn from the deleterious part of the DFE (i.e., if  $z = 0$ ) or from the exponential beneficial

156 tail (i.e., if  $z = 1$ ). The parameters  $\hat{\sigma}$ ,  $\hat{\lambda}$ , and  $\hat{x}$  are estimated from the underlying experimental  
157 data, and based on growth rate estimates obtained from OLS linear regression.

158 Finally, the accuracy of the parameter estimates was assessed by computing the mean squared  
159 error (MSE)

$$160 \text{MSE} = \frac{1}{K-1} \sum_{i=2}^K (\hat{r}_i - r_i)^2,$$

161 the length of the credibility interval (CI, calculated from the MCMC posterior distribution),  
162 and the frequency of the true growth rate lying in the 95% confidence interval calculated over  
163 100 simulated data sets.

#### 164 *Outlier detection in empiricIST*

165 Apart from its main program – the Bayesian MCMC program – *empiricIST* provides Python  
166 and shell scripts for data pre- and post-processing. Details about their usage and options are  
167 given in the accompanying manual. Here we outline the two different options that are available  
168 for dealing with outliers in the sequencing data – i.e., outlier detection and data imputation –  
169 and explain the DFE tail-shape estimation (see Outlier Detection in *empiricIST* in SI).

170 As an alternative to treating outliers as unobserved (i.e., missing data), we also implemented an  
171 approach in which data points identified as outliers were imputed (see SI). For that we again used  
172 the linear regression of the log ratios of the mutant’s read number to the total number of reads at  
173 each individual time point (i.e., the ‘total’ normalization, *sensu* Bank *et al.*, 2014), and classified  
174 as outliers data points that exceed the DFBETA cutoff of 2 and that had an absolute studentized  
175 residual bigger than 3 . In comparison to other reasonable and established outlier criteria, this  
176 approach proved to be more cautious as exemplified by the higher specificity and lower sensitivity  
177 (Fig. 2, Fig. S1). By combining two independent outlier criteria (i.e., the DFBETA statistic  
178 and the studentized residuals), this approach ensures that data points identified as outliers have  
179 leverage effects (i.e., change the slope considerably) and are in conflict (meaning that are very  
180 different in comparison) with the remaining data points. Thus, to minimize changes in the  
181 original experimental data we took an extremely conservative approach, such that only those  
182 data points that stand out as extreme outliers will be imputed.

183 When comparing the mean squared error (MSE) over 100 simulated data sets across different  
184 outlier detection methods, we find that the MSE increases with the proportion of outliers in the  
185 data set, independent of the method used. Imputing data points generally improves the accuracy

186 of the parameter estimates compared to treating outliers as missing data (Bank *et al.*, 2014, ;Fig.  
187 S2, S3). Expectedly, when there are no outliers in the data, the wild-type normalization displays  
188 the lowest error. However, with only 1% outliers in the data, the error of the wt-normalization is  
189 comparable to that of the total normalization and becomes increasingly worse as the proportion  
190 of outliers in the data increases (Fig. S2). Note that in the presence of outliers, using any outlier  
191 method improves growth rate estimates considerably.

### 192 *Estimating the shape for the beneficial tail with empiricIST*

193 Finally, *empiricIST* contains a Python script for estimating the shape of the beneficial tail of  
194 the DFE. Currently, it is believed that these effects typically follow an exponential distribution  
195 (Gillespie, 1983, 1984) characterized by many small, nearly neutral mutations and a few strongly  
196 beneficial mutations. Using extreme value theory, it is however possible to test whether experi-  
197 mental data complies with that assumption (and falls into the Gumbel domain), or whether the  
198 data is better represented by distributions from the Weibull domain (i.e., distributions that de-  
199 cay more rapidly as an exponential distribution, implying more small-effect mutations) or from  
200 the Fréchet domain (i.e., distributions decaying less rapidly than an exponential distribution  
201 implying an excess of large-effect mutations; see also Beisel *et al.*, 2007). Additional information  
202 about the different types of distributions and likelihood estimation are available in the section  
203 on DFE estimation in the SI.

204 We analyzed the power of the maximum-likelihood method to make this distinction by simulating  
205 1000 Generalized Pareto Distribution (GPD) data sets for different underlying shape parameter  
206 ( $\kappa$ ) values (spanning across all three GDP domains) and varying sample sizes. We find that  
207 for small sample sizes (Fig. S4A, B)  $\hat{\kappa}$  displays a large variance and a slight negative bias, in  
208 particular, if the underlying shape parameter is from the Weibull domain (i.e.,  $\kappa < 0$ ). This bias  
209 is caused by a (numerical) discontinuity in the log-likelihood function around  $\kappa = -1$  (eq. S3 in  
210 SI), causing  $\kappa$  to consistently deviate (Rokyta *et al.*, 2008). As sample size increases, however,  
211 the variance of the maximum-likelihood estimate decreases and its bias vanishes (Fig. S4C, D).  
212 Furthermore, while  $\kappa$  typically falls into the correct domain (even for low sample sizes), the  
213 statistical power for detecting deviations from the null hypothesis (i.e., whether  $H_0: \kappa = 0$ ) is low  
214 (unless sample sizes are large).

## 215 **2.2 Experimental data**

216 The data used in this study were originally obtained in Bank *et al.* (2014) using the EMPIRIC  
217 approach (Hietpas *et al.*, 2011, 2012). In this study, all 576 possible single-codon mutations  
218 in a 9 amino-acid region of the C terminal part of Hsp90 in *Saccharomyces cerevisiae* were  
219 generated and bulk competitions were performed under six different environmental conditions  
220 (25°C, 30°C, 36°C, 25°C + S, 30°C + S, and 36°C + S, where S represents the addition of 0.5M  
221 sodium chloride). For simplicity, we will refer to these conditions as normal medium or high  
222 salt medium, and abbreviate these by 25N and 25S, for example, when additionally referring to  
223 the 25°C environment. The experiment was replicated 3 times for the 30N environment and 2  
224 times for the 30S environment. Populations were originally adapted to the 30N environment,  
225 thus changes to other environments correspond to shifts from the optimum (Bank *et al.*, 2014).  
226 Growth rates for all mutants were estimated using *empiricIST*. Furthermore, to obtain growth  
227 rate estimates per amino-acid (residue) position, we pooled nucleotide sequences and jointly  
228 estimated growth rates for those nucleotide sequences that resulted in the same amino-acid  
229 sequence (see above and SI). Our downstream analyses are based on 1000 subsamples of the  
230 posterior distribution obtained from *empiricIST*, if not otherwise indicated. Selection coefficients  
231 were obtained by normalizing to the median growth rate of all mutations synonymous to the  
232 reference sequence as detailed in Bank *et al.* (2014).

### 233 *Distribution of synonymous mutations*

234 We obtained the distribution of synonymous fitness effects (DSE) across all amino-acid mutations  
235 as the difference between each individual codon selection coefficient and its corresponding pooled  
236 amino-acid estimate. These data were used to perform the analyses in the section on potential  
237 mechanisms underlying the effect of synonymous mutations on fitness.

## 238 **2.3 Detecting the effect of synonymous mutations**

### 239 *Analyses and results to assess experimental error and reproducibility of measurements*

240 To assess the reproducibility of measurements, we compared the correlation between selection  
241 coefficient estimates across the three 30N and two 30S replicates, and computed the overlap  
242 in their growth rate posteriors. For each replicate pair, we calculated the correlation between  
243 mutation-specific fitness effects from both the median estimates and 1000 randomly selected

244 posterior samples. The median correlation of fitness effects across pairs of replicates was 0.84  
245 (lower and upper credibility intervals from 1000 posterior samples: [0.78, 0.88]) for high salt  
246 medium and was 0.98 (lower and upper credibility intervals from 1000 posterior samples: [0.97,  
247 0.99]) in standard medium (Fig. S5) confirming that the experimental protocol has an excellent  
248 resolution for measuring selection coefficients. An ANOVA test indicated that experimental  
249 error was negligible in comparison to the effect of changing medium (Table S1, Fig. S6) and  
250 confirmed the previously observed strong costs of adaptation (Hietpas *et al.*, 2013).

251 To quantify whether the *empiricIST* credibility intervals cover the experimental error appropri-  
252 ately, we estimated the overlap between the 95% credibility intervals of the posterior distribution  
253 for all pairs of replicates. We observed a large overlap between pairs of replicates (Fig. S7, nor-  
254 mal environment – a) Rep1-2: 98%; b) Rep1-3: 91%; c) Rep2-3: 90%; high salt environment –  
255 d) Rep1-2: 90%), indicating that the variance between replicates is indeed mostly covered by  
256 variance in the posterior distribution, and that we can use *empiricIST* credibility intervals as  
257 confidence levels in our analysis.

258 We used linear models to extract the contribution of various factors to the estimated effects  
259 of synonymous mutations. Model variable names are highlighted throughout the paper using  
260 Italics. The following analyses were performed on the distribution of synonymous effects data,  
261 i.e., the data in which the median amino-acid effect was removed.

262 We estimated the relative contributions of the experimental error and the effect of synonymous  
263 mutations in the data by means of three approaches. First, we compared the impact of *replicate*,  
264 *codon* and *medium* (i.e., whether salt was added or not) using the following ANOVA model with  
265 data between replicates 2 and 3 of both the standard and the high salinity environment for 30C:

$$\begin{aligned} Y &= \text{codon} + \text{replicate} + \text{medium} + \text{replicate}*\text{codon} + \text{codon}* \text{medium} \\ &+ \text{replicate}* \text{medium} + \text{codon}* \text{medium}* \text{replicate} \end{aligned}$$

266 where Y corresponds to the normalized selection coefficient, *codon* to a fixed factor corresponding  
267 to the 64 codons present in the data, *replicate* to a fixed factor pertaining to the arbitrary  
268 replicate number 2 or 3 for each environment, *medium* is a fixed factor corresponding to the  
269 presence or absence of high salt concentration in the medium and  $\epsilon$  corresponds to the residual  
270 error. We estimated effect size by calculating  $\eta^2$  (i.e., the ratio of the variance explained by a  
271 predictor to the total variance explained by the entire model - (Levine and Hullett, 2002)) for  
272 each of the model terms, using the *etasq* function of the *R* package *sjstats* (Lüdecke, 2017). To

273 assess the variability of our estimates, we performed the analysis for 1000 posterior samples.  
274 Finally, using the distribution of synonymous mutations referred above, we tested the overlap  
275 of beneficial mutations across replicates for normal and high salinity environments. For that,  
276 we extracted the 30 most beneficial synonymous mutations (approximately corresponding to the  
277 5% beneficial tail) for each replicate, and estimated the overlap across the three 30N replicates,  
278 and two 30S replicates.

#### 279 *Quantifying the effect size of synonymous mutations*

280 To quantify the effect size of codon changes, we performed a linear regression for each amino-  
281 acid (including all amino-acids with 3 or more codons) and calculated  $\eta^2$  (as proxy for effect size  
282 (Levine and Hullett, 2002)) for the *codon* term. The regression per amino-acid was performed  
283 within each environment and took into account *residual depth* (i.e., whether the position was  
284 buried or exposed). Pooling of positions was done to allow for the testing of codon effect within  
285 amino-acid. To minimize potential differences arising from pooling positions, we separated the  
286 data into buried and exposed positions according to residue depth. Additionally, using an  
287 ANOVA model we tested how the estimated effect size per amino-acid (using  $\eta^2$  as dependent  
288 variable) varied across *environment* and *amino-acid*.

289 Finally, we calculated 10 000 pairwise differences between synonymous mutations, between ran-  
290 dom amino-acid pairs and between random pairs of samples of the posterior to assess the effect  
291 of synonymous mutations in comparison with amino-acid changes and in comparison to the  
292 variation between posterior samples.

#### 293 *Investigating the effect of synonymous mutations on the topography and the dynamics of adaptive* 294 *walks in codon fitness landscapes*

295 To quantify the impact of effects of synonymous mutations coding for the same amino-acid  
296 on the topography of the fitness landscape, we compared the single-effect landscape with the  
297 averaged landscape. For the single-effect landscapes (Fig. 1D) the effect of each codon was  
298 directly obtained from the experimental data. For the averaged landscape (Fig. 1C) we assigned  
299 to every codon that coded for the same amino-acid the same pooled amino-acid estimate obtained  
300 from *empiricIST*.

301 Each amino-acid position in our data set corresponds to a complete multi-allelic fitness landscape  
302 with  $3^4 = 64$  genotypes. We characterized the resulting  $9 \cdot 6 = 54$  fitness landscapes using several  
303 fitness landscape statistics. We estimated 1) the roughness-to-slope ratio (Aita *et al.*, 2001;

304 Szendro *et al.*, 2013; Bank *et al.*, 2016) to quantify the relative deviations from an additive model;  
305 2) the multi-allelic gamma statistics (Bank *et al.*, 2016; Ferretti *et al.*, 2016) to characterize the  
306 prevalence and type of epistasis in the landscape; 3) the number of local peaks (Szendro *et al.*,  
307 2013); and 4) the length and variance in the length of potential adaptive walks in the landscapes  
308 (Neidhart and Krug, 2011; Szendro *et al.*, 2013).

309 Credibility of the estimates was assessed by computing the fitness landscape statistics for 100  
310 posterior samples.

### 311 *Potential mechanisms underlying the effect of synonymous mutations on fitness*

312 There are several mechanisms through which synonymous mutations can affect protein trans-  
313 lation (reviewed in Plotkin and Kudla, 2011). In this study we focused on whether codon  
314 usage frequency or predicted mRNA stability (using as proxy Gibbs free energy and melting  
315 temperature) can predict effects of synonymous mutations (Presnyak *et al.*, 2015).

316 Firstly, to enable the inclusion of codon frequency patterns in yeast into our regression models,  
317 we obtained the relative abundance of each codon in the yeast genome from the Codon Usage  
318 Database (<http://www.kazusa.or.jp/codon/cgi-bin/showcodon.cgi?species=4932>).

319 Secondly, synonymous mutations may affect translation through different stability of the mRNA  
320 generated by different codons. To obtain predictions of how mRNA stability is affected by  
321 synonymous mutations, we ran the prediction software *mfold* (Zuker *et al.*, 1999; Markham  
322 and Zuker, 2008), for 25°C, 30°C and 36°C and with high salt concentrations (0.5M Na<sup>+</sup>),  
323 with physiological concentrations of salt (0.015M Na<sup>+</sup>), and 0.001 M Mg<sup>2+</sup>, respectively. As  
324 input, we used sequences spanning 135 nucleotides of the Hsp90 protein in yeast. To obtain  
325 these sequences, we added 54 nucleotides flanking both 5' and 3' sides of the region of interest  
326 (complete sequences were obtained from <https://www.addgene.org/41188/sequences/>). From  
327 each of these data sets, we selected the conformation with the lowest Gibbs free energy (dG) or  
328 with the highest melting temperature (T<sub>m</sub>), as highest-stability reference points.

329 Since Hsp90 is a chaperone protein involved in the response to thermal stress as well as in the  
330 regulation of osmotic stress (Yang *et al.*, 2006; Boucher *et al.*, 2014), we tested the impact of each  
331 factor in each environment and amino-acid position and quantified how variation in temperature,  
332 osmotic stress and residue position affected the correlation between *mRNA melting temperature*,  
333 *codon frequency* and *Gibbs free energy* and the effect of synonymous mutations. We used the  
334 following models:

$$Y = \text{melting temperature} + \epsilon$$

$$Y = \text{codon frequency} + \epsilon$$

$$Y = \text{Gibbs free energy} + \epsilon$$

$$Y = \text{temperature} + \text{salt} + \text{residue position} + \text{codon frequency} + \text{Gibbs free energy} \\ + \text{melting temperature} + (\dots) + \text{temperature} * \text{salt} * \text{residue depth} * \text{codon frequency} \\ * \text{Gibbs free energy} * \text{melting temperature} + \epsilon$$

335 where  $Y$  corresponds to the fitness effect of synonymous mutations (see above), *temperature* is  
336 a covariate coding for 25°C, 30°C and 36°C, *salt* is a fixed factor that codes for the presence or  
337 absence of added salt in the medium, *residue position* relates to the residue position in the amino-  
338 acid sequence (582 to 590), *codon frequency* is the frequency of each codon in the genome (see  
339 above), *Gibbs free energy* is the variation in Gibbs free energy obtained from mfold and *melting*  
340 *temperature* the melting temperature for the RNA estimated through mfold. We included all  
341 interactions between the studied factors in the model. The effect size of each term in the model  
342 was estimated through the  $\eta^2$  (Levine and Hullett, 2002) for 1000 posterior samples.

343 All analyses were performed with R (R version 3.3.3) (R Core Team, 2017) or Mathematica  
344 11 (version 11.2) (Wolfram Research, Inc., 2017). The complete documentation of all analyses,  
345 which allows for the reiteration of all steps, is available as Online Supplementary Material.

### 346 **3 Results & Discussion**

347 We implemented a software to infer selection coefficients from deep mutational scanning exper-  
348 iments. The *empiricIST* software is based on a previously developed Bayesian Markov chain  
349 Monte Carlo (MCMC) approach (Bank *et al.*, 2014), and is a user-friendly and accurate soft-  
350 ware for improved growth rate estimation from time-sampled deep-sequencing data. We took  
351 advantage of the high accuracy provided by this method to estimate selection coefficients for  
352 synonymous mutations.

### 3.1 Bayesian MCMC outperforms linear regression

Validating the method with various types of pseudo-data shows that our MCMC generally outperforms the ordinary least square regression (OLS). Figures 2 and S1 show the results for the standard and the data-based simulations (see Material & Methods). Although the mean square error (MSE) of the MCMC is comparable to that of the OLS when analyzing few time points (i.e., 3 to 5 time points), the MSE of the MCMC decreases faster as the number of time points increases (Fig. 2A).

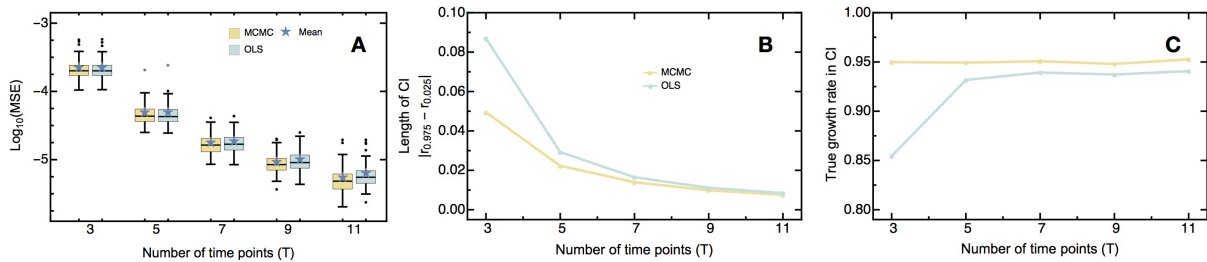


Figure 2: **Comparison between performance of *empiricIST* and ordinary least square regression with varying number of time points sampled.** A) mean square error (MSE), B) size of the credibility interval (CI), and C) the proportion the true growth rate contained in the CI. As shown, *empiricIST* shows equal or lower MSE than OLS regression, particularly as the number of sampled time points increases. Furthermore, *empiricIST* outperforms the OLS regression in terms of the size of the CI and in capturing the true growth rate, even when sampling a small number of time points.

Furthermore, when analyzing few time points, the length of the credibility interval (CI) is significantly smaller for the MCMC than the corresponding confidence interval of the OLS regression (Fig 2B). While the difference between the length of the confidence intervals decreases as the number of time samples  $T$  increases, the size of the CI from the MCMC always remains smaller, which implies that it delivers more precise and accurate results than the conventional OLS regression. Most importantly, and unlike the OLS regression, the CI of the MCMC remains well calibrated along the entire range of parameters (Fig. 2 C), despite being generally narrower than its OLS counterpart.

### 3.2 Synonymous mutations have detectable effects on fitness

Previous studies have shown that synonymous mutations can directly affect fitness (e.g. Lind *et al.*, 2010; Firnberg *et al.*, 2014; Hunt *et al.*, 2014) and impact the ability of populations to adapt to new environments (Bailey *et al.*, 2014; Agashe *et al.*, 2016). For example, Bailey *et al.* (2014) found that two synonymous mutations were driving adaptation to a new medium in two experimental replicates by increasing the expression of a gene involved in glucose metabolism.

374 In a more recent study, Agashe *et al.* (2016) found that the deleterious effect of synonymous  
375 mutations in a medium with methylamine as the sole carbon source could be rescued by differ-  
376 ent mutations, including four synonymous mutations that increased transcription and protein  
377 production levels. The impact of synonymous mutations at the genome wide level can also be  
378 found in patterns of codon usage bias (synonymous codons are used in different frequencies)  
379 across genomes. Evidence coming from studies within and between species support the role of  
380 direct selection on synonymous sites in various genes (DuMont *et al.*, 2004; Singh *et al.*, 2007;  
381 Hershberg and Petrov, 2009; Ran and Higgs, 2010; Shah and Gilchrist, 2011; Choi and Aquadro,  
382 2016; Sun *et al.*, 2016). A first piece of evidence for synonymous effects in the studied region of  
383 Hsp90 came from Bank *et al.* (2014), who reported that one of the 15 mutations synonymous  
384 to the parental sequence had a significantly deleterious effect in 4 out of 6 environments (Fig. 9  
385 Bank *et al.*, 2014). In order to evaluate the effects of synonymous mutations on a larger scale,  
386 we applied the *empiricIST* software to the data set from Bank *et al.* (2014), which consists of  
387 bulk competitions of all 576 possible single codon-changing mutations in a 9 amino-acid region  
388 of Hsp90 in *Saccharomyces cerevisiae* across 6 different experimental conditions. For the envi-  
389 ronments 30N and 30S (30°C with normal and high salinity) we confirmed our results across  
390 the available 3 and 2 replicates, respectively. To quantify the effect of synonymous mutations as  
391 compared with the effect of non-synonymous mutations and experimental error we estimated the  
392 absolute pairwise difference between random pairs of amino-acids, codons, posterior samples and  
393 replicates (Table S2, see Material & Methods). On average, the effects of synonyms are small,  
394 but larger than the experimental error. In fact, 11% of the synonymous mutations present in  
395 the 5% beneficial tail (normalized to the effect of each amino-acid, see Material & Methods) are  
396 common between the three 30N replicates and 11% between the two 30S replicates, as compared  
397 with 0.0125% vs. 0.025% overlap expected by chance. The median pairwise difference between  
398 two synonymous mutations was between 3% (in 25S) and 27% (in 36N) larger than the difference  
399 between two draws from the posterior of the same codon (Table S2). As expected, the average  
400 effect of synonymous mutations is much smaller than that of non-synonymous mutations (Table  
401 S2). The estimated average fitness difference between two synonymous mutations is between  
402 13% (in 36N) to 32% (in 25S) of the difference between two non-synonymous mutations. In  
403 concordance with these estimates, a one-way ANOVA shows that 20-30% of the fitness changes  
404 within amino-acids can be explained by codon variation alone (see Fig. S8). On average, the  
405 effects of synonymous mutations are higher in the 36N environment (Table S2, Fig. S8), where  
406 Hsp90 is expected to be more important for organism survival (Yang *et al.*, 2006; Boucher *et al.*,

408 **3.3 The beneficial tail of the distribution of synonymous fitness effects**

409 The distribution of fitness effects contains information about the availability of beneficial mu-  
 410 tations (Orr, 2005, 2010). It is of particular interest to study the shape of the beneficial tail of  
 411 this distribution as it determines various aspects about the nature of adaptive walks (Orr, 2010;  
 412 Eyre-Walker, 2006). Bank *et al.* (2014) previously found that for all of the environments, except  
 413 for 25S, the beneficial tail of the full distribution of fitness effects most likely belonged to the  
 414 Weibull domain. This suggested that populations were close to a well-defined optimum, and the  
 415 available beneficial mutations would be of similar and small size (Orr, 2010; Joyce *et al.*, 2008;  
 416 Bank *et al.*, 2014).

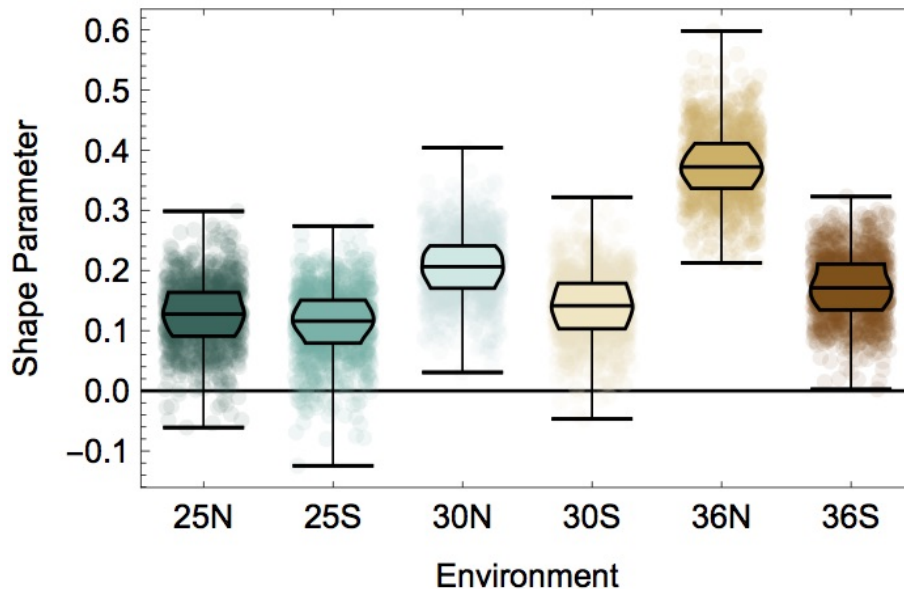


Figure 3: **Distribution of the shape parameter of the beneficial tail of synonymous mutations.** The shape parameter was estimated using the tail shape estimator from *empiricIST* and used the information of 1000 samples of the posterior distribution. In all the environments, the shape of the tail is clearly positive indicating that it belongs to the Fréchet domain. This implies that most mutations in this distribution will be characterized by nearly neutral effects. Environmental conditions are indicated by the combination of temperature (25C, 30C and 36C) and salinity (N = normal and S = high salinity).

417 We used the tail shape estimator from the *empiricIST* software to estimate the tail shape of  
 418 the distribution of beneficial synonymous mutations. To obtain this distribution, we subtracted  
 419 the average amino-acid effect from the selection coefficient of each codon. We find that the  
 420 shape parameter of the fitted Generalized Pareto Distribution (GPD) is most likely positive  
 421 in all environments, which indicates that the resulting shape of the beneficial tail is likely to

422 belong to the Fréchet domain (Fig. 3) (Orr, 2010; Joyce *et al.*, 2008). Distributions from this  
423 domain are characterized by many mutations of small effect, along with few mutations of large  
424 and unpredictable effect (Joyce *et al.*, 2008; Neidhart and Krug, 2011; Jain and Seetharaman,  
425 2011). This is consistent with the expectation that most synonymous mutations in the whole  
426 data set have little effect on fitness, but some have large fitness effects.

### 427 **3.4 Synonymous mutations affect the topography of the landscape**

428 We investigated the effect of synonymous mutations on the topography of the fitness landscape  
429 by comparing averaged and single-effect landscapes (see Fig. 1 C, 1 D, Material & Methods) for  
430 each of the 9 amino-acid positions across 6 environments. For all 54 landscapes, we computed  
431 two statistics: the roughness-to-slope ratio  $r/s$  (Szendro *et al.*, 2013) and the locus-specific  
432 gamma statistic (Ferretti *et al.*, 2016). The roughness-to-slope ratio describes the prevalence  
433 of epistasis (i.e., the extent of non-linear fitness effects between mutations) in relation to the  
434 magnitude of fitness effects in the landscape (Carneiro and Hartl, 2010; Schenk *et al.*, 2013).  
435 The  $\gamma_{i \rightarrow j}$  statistic measures the correlation of fitness effects of the same mutations in a single-  
436 step distance across all genetic backgrounds. Whereas the roughness-to-slope ratio describes  
437 the landscape by means of only two values,  $\gamma_{i \rightarrow j}$  results in a detailed fingerprint of the fitness  
438 landscape that makes heterogeneity of epistasis in the landscape visible. In general all landscapes  
439 are highly epistatic ( $r/s > 1$ ), with the magnitude of the roughness-to-slope ratio depending  
440 on amino-acid position and environment (Fig. S9). Single-effect landscapes are slightly more  
441 epistatic (higher ratio) than averaged landscapes, although this difference is in general small. In  
442 high salinity, the difference in the  $r/s$  ratio between amino-acid positions and between averaged  
443 and single-effect landscapes is larger (Fig. S9). The increased epistatic signal observed in these  
444 environments could be caused by the combination of low absolute growth rates observed in  
445 high salinity conditions (c.f. Table 1 in Bank *et al.*, 2014) and larger experimental uncertainty  
446 (S7) in this environment. This indicates that one should be cautious when interpreting the  
447 roughness-to-slope ratio across data sets, because it may be reflecting differences in growth  
448 rates and experimental error between environments, rather than genuine changes in the epistatic  
449 component of the landscape. Computing the  $\gamma_{i \rightarrow j}$  statistic shows that averaged and single-effect  
450 landscapes tend to display the same type of epistasis within amino-acid position and environment  
451 (Fig. 4, Fig. S10). In general, magnitude and sign epistasis (when the effect and sign of a  
452 mutation depends on the genetic background where it appears) are prevalent and we observe

453 only few cases of reciprocal sign epistasis (both mutations switch sign when combined; Fig. S10).  
454 Since reciprocal sign epistasis is a necessary, but not a sufficient condition for multiple fitness  
455 peaks in a landscape (Poelwijk *et al.*, 2011), its low prevalence suggests that there should be few  
456 fitness peaks in both averaged and single-effect landscapes. In contrast to the results from the  
457 roughness-to-slope ratio, the  $\gamma_{i \rightarrow j}$  statistic shows smaller differences between environments. As  
458 this statistic computes results based on the correlation and not the effect size of fitness effects  
459 across genetic backgrounds, it is less sensitive to variation in growth rates and experimental  
460 error. In fact, most differences in the type of epistasis are found when comparing the order  
461 in which mutations occur. In particular, landscapes resulting from non-synonymous mutations  
462 ( $\gamma_{1 \rightarrow 2}$ ,  $\gamma_{2 \rightarrow 1}$ ) display in general strong epistasis (Fig. 4), compared to landscapes that include  
463 synonymous mutations ( $\gamma_{1 \rightarrow 3}$ ,  $\gamma_{2 \rightarrow 3}$ ,  $\gamma_{3 \rightarrow 1}$ ,  $\gamma_{3 \rightarrow 2}$ ). However, the presence of magnitude/sign  
464 epistasis in both  $\gamma_{3 \rightarrow 1}$ ,  $\gamma_{3 \rightarrow 2}$  landscapes suggests that synonymous mutations do not have the  
465 same effects across different amino-acids. Similar to what was observed in the roughness-to-slope  
466 ratio, there is variation across amino-acid positions for both non-synonymous and synonymous  
467 mutations.. Thus, the structure of the codon table (i.e., the existence of synonymous and non-  
468 synonymous mutations) imposes a strong general pattern of epistasis on the landscape. However,  
469 variation in this pattern across positions and environments indicates that every single amino-acid  
470 position has indeed a differently shaped fitness landscape.

### 471 3.5 Impact of synonymous mutations on adaptive walks

472 Including synonymous mutations changes the topography of the landscape, which may affect the  
473 accessibility of different mutational paths by creating additional peaks and sinks in the fitness  
474 landscape. To quantify the impact of synonymous effects on adaptive walks, we calculated  
475 the number of optima, the mean expected length of adaptive walks, and the variance in the  
476 number of steps for the single-effect and averaged landscapes. We based our calculation on  
477 the assumption of the strong-selection weak-mutation limit (Gillespie, 1984), in which evolution  
478 happens by means of sequential mutational changes that result in an adaptive walk that ends  
479 in a fitness peak (e.g. Orr, 2005; Schoustra *et al.*, 2009; Frank, 2014; Zagorski *et al.*, 2016).  
480 We define a fitness peak as any genotype with fitness higher than all single-step mutational  
481 neighbors. For averaged landscapes, in which all synonymous mutations are assigned equal  
482 fitness, we consider a fitness plateau spanned by synonymous codons as a single local optimum  
483 if all non-synonymous codons in a distance of a single nucleotide step have lower fitness (as in

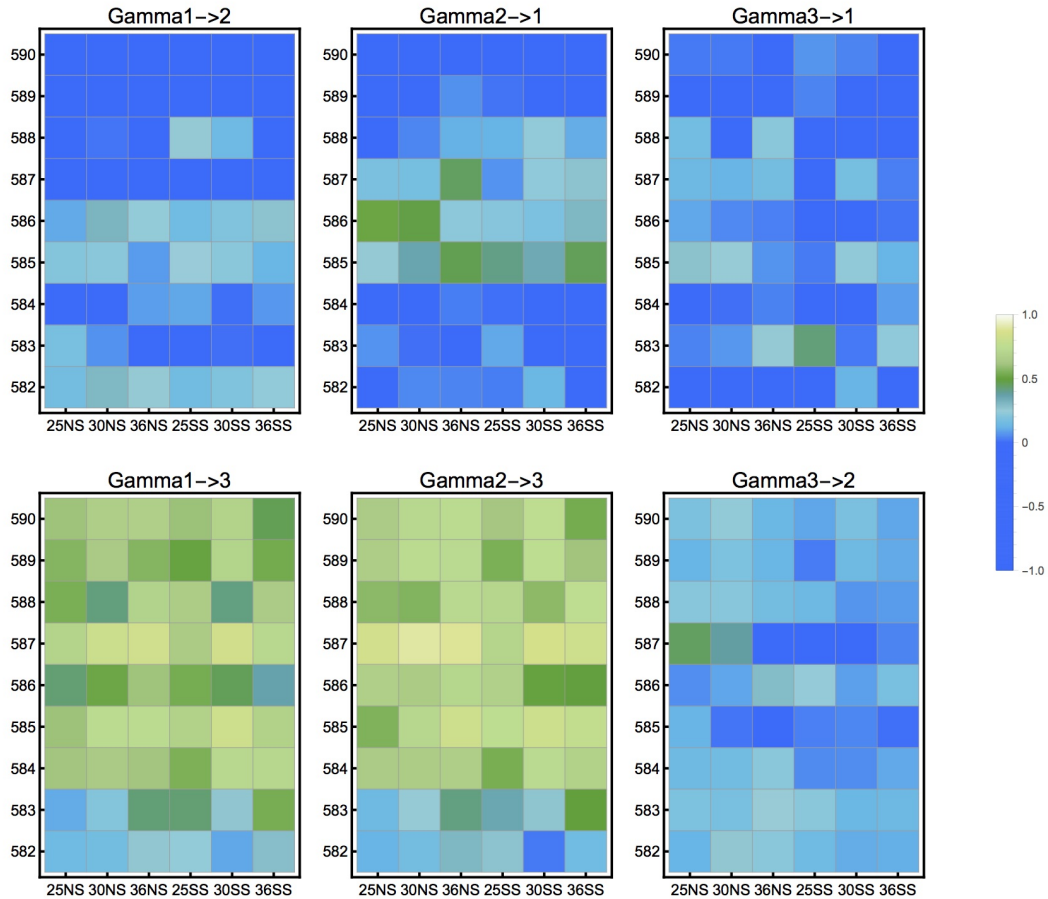


Figure 4: **Gamma statistic calculated for pairs of mutations in different codon positions for single-effect landscapes for the 9 amino-acid positions studied (y-axis) in the different environments (x-axis).** In general, non-synonymous mutations on top of each other ( $\gamma_{1\rightarrow 2}$ ,  $\gamma_{2\rightarrow 1}$ ) show prevalence of sign epistasis ( $\gamma$  between 1 to  $-1/3$ ), while non-synonymous mutations on top of synonymous mutations ( $\gamma_{1\rightarrow 3}$ ,  $\gamma_{2\rightarrow 3}$ ) show higher prevalence of magnitude epistasis ( $\gamma$  between 1 and 0). There is no clear variation across environments (x axis), but we find a clear impact of amino-acid position in the type of epistasis (y axis). Interestingly, both  $\gamma_{3\rightarrow 1}$  and  $\gamma_{3\rightarrow 2}$  indicate a potential epistatic hotspot in positions 582 and 583 across all environments.

484 Fig. 1 C). By definition, the number of fitness peaks in the averaged landscape has to be lower  
 485 or equal to that of the single-effect landscape. Indeed, we find that there is usually a large  
 486 difference in the number of fitness peaks between single-effect and averaged landscapes (Fig. 5,  
 487 Fig. S11). This difference is environment-dependent and also varies across amino-acid positions  
 488 (Fig. 5, Fig. S11). The variation in the differences between single-effect and averaged landscapes  
 489 is not consistent within buried or exposed positions (see Material & Methods), which suggests  
 490 that the impact of synonymous mutations is not due solely to effects at the structural level of  
 491 the protein. In contrast to what was expected due to the reduced number of observed peaks, we  
 492 observe shorter and less variable adaptive walks for averaged landscapes than for single-effect

493 landscapes (Fig. S12, Fig. S13). This suggests that evolution on the ‘true’ landscape that  
494 includes effects of synonymous mutations is less predictable (Lobkovsky *et al.*, 2011; De Visser  
495 and Krug, 2014), and that it may stall at an intermediate optimum created by variation in  
496 synonymous fitness effects. Different environments leave a stronger signature in single-effect  
497 landscapes than in averaged landscapes. In fact, for most environments and positions, averaged  
498 landscapes show only 1 or 2 optima in the landscape (Fig. 5, Fig. S11). Conversely, among the  
499 single-effect landscapes the 25°C stands out with a large number of peaks, coupled with short  
500 adaptive walks (Fig. S12). This could reflect the lower constraint on Hsp90 function at low  
501 temperatures, as well as the lower absolute growth rates of the population under this condition  
502 which may open up more opportunities for adaptation. In further support for this hypothesis,  
503 we observe fewer optima and longer and more variable adaptive walks at 36N, which is in  
504 agreement with the importance of Hsp90 under high temperatures (Hietpas *et al.*, 2013; Bank  
505 *et al.*, 2014; Boucher *et al.*, 2014; Mishra *et al.*, 2016). This is consistent with the small number  
506 of beneficial mutations observed by Bank *et al.* (2014) under this condition. This points to a  
507 scenario in which there is increased evolutionary constraint, such that the number of solutions  
508 to the adaptive challenge is very limited.

509 Our results allow for an interesting thought experiment regarding the impact of synonymous  
510 mutations on evolution across populations of different sizes. The average small differences in  
511 synonymous effects observed here will be only be visible to selection in large populations, where  
512 they may frequently stall adaptation if the population gets trapped in a local fitness peak.  
513 Bottlenecks (i.e., sudden drops in the population size), which can occur under natural scenarios  
514 and are also frequently imposed in experiments, may render synonymous mutations effectively  
515 neutral and thus erase the difference between averaged and single-effect landscapes. By opening  
516 mutational paths and bridging fitness peaks, a (temporally) smaller population size could thus  
517 speed up adaptation and increase its predictability (Wright, 1931; Jain *et al.*, 2011). This effect,  
518 even if weak, would be in contrast to the slow down of adaptation and decrease of predictability  
519 of evolution in small populations proposed in standard population-genetic theory (Orr, 2000;  
520 Lanfear *et al.*, 2014).

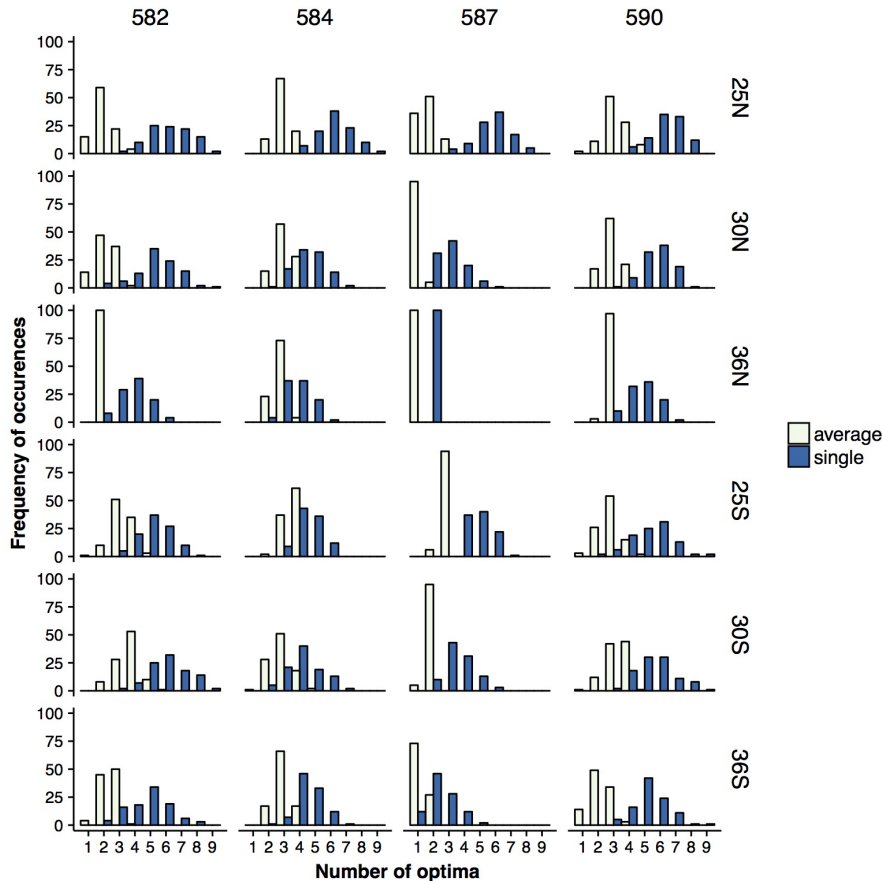


Figure 5: **Figure 5: Number of optima observed from 100 posterior samples of single-effect (dark blue) and averaged (light yellow) landscapes for positions 582, 584, 586 and 590 (from left to right) across environments.** The number of optima is always higher in single-effect than in averaged landscapes across environments. The number of optima is smaller at high temperatures, which may indicate increased constraints to adaptation. The large difference between the number of peaks in averaged and single landscapes suggests that synonymous mutations can affect adaptation to a new environment by trapping the population in a local optimum.

### 521 3.6 Effects of synonymous mutations are driven by a combination of mecha- 522 nisms

523 Synonymous mutations can affect fitness by altering speed and accuracy of translation, and  
524 mRNA folding and stability (Drummond and Wilke, 2008; Kudla *et al.*, 2009; Zhou *et al.*,  
525 2009; Sharp *et al.*, 2010; Plotkin and Kudla, 2011; Shabalina *et al.*, 2013; Presnyak *et al.*, 2015;  
526 Yu *et al.*, 2015; Knöppel *et al.*, 2016; Brule and Grayhack, 2017). It has been proposed that  
527 protein folding may be affected more significantly by changes in translation accuracy for buried  
528 (structural) positions, as they are often involved in the formation of crucial secondary and  
529 tertiary structures of the protein (Drummond and Wilke, 2008; Zhou *et al.*, 2009; Saunders  
530 and Deane, 2010). We evaluated whether the effect of synonymous mutations that we observe

531 can be explained by variation in codon preference or mRNA stability. For that, we analyzed  
532 a full linear model incorporating temperature, medium composition, residue position, Gibbs  
533 free energy, melting temperature of mRNAs, and codon usage frequency, as well as all possible  
534 interactions of those factors. We also estimated the slopes of linear regressions for each predictor  
535 to quantify the contribution of these factors to the fitness effects of synonymous mutations for  
536 each environment and amino-acid position. As may be expected, considering the diverse amino-  
537 acid positions and environments studied, no clear predictors of codon fitness emerged. We found  
538 fitness effects of synonymous mutations to be affected by interactions between residue positions  
539 and temperature, medium composition, mRNA melting temperature and Gibbs free energy,  
540 and codon usage frequency (Table S3). In addition, we saw a clear impact of residue position  
541 and temperature in the fitness effects of synonymous mutations (Table S3, Fig. S14). Despite  
542 generally weak correlations between fitness effects and the predictors ( $r^2$  for codon frequency:  
543 0.0235,  $r^2$  for Gibbs free energy: 0.0217,  $r^2$  for melting temperature: 0.0246), correlations tended  
544 to be stronger at higher temperatures in standard medium (Fig. S15). Namely, we observed  
545 that in 36N there is a deleterious effect of higher mRNA stability for positions 585 and 587,  
546 and a beneficial effect of higher mRNA stability for positions 583 and 584 (Fig. S15b,S15c). At  
547 this temperature, more common codons show beneficial effects at positions 586, 587 and 590,  
548 and negative effects at positions 583, 585 and 588. This indicates that the impact of mRNA  
549 stability and codon frequency on the fitness effects of synonymous mutations is dependent on  
550 residue position and environment. The usage of different synonymous codons allows cells to  
551 slow down or arrest protein production in response to sudden environmental changes and to  
552 optimize resource production (Zhang *et al.*, 2009; Fredrick and Ibba, 2010; Tuller *et al.*, 2010).  
553 Our results suggest that a combination of several mechanisms drives the effects of synonymous  
554 mutations. Namely, we found a correlation of fitness effects of synonymous mutations with  
555 mRNA stability and codon frequency. This is in line with other studies demonstrating that  
556 synonymous codons affect mRNA stability (Hilgers, 2006; Romero and Arnold, 2009; Presnyak  
557 *et al.*, 2015) by modulating protein translation kinetics through optimal codon usage (Akashi,  
558 1994; Drummond and Wilke, 2008; Presnyak *et al.*, 2015; Harigaya and Parker, 2016). However,  
559 synonymous mutations do not show consistent effects within buried (586 to 590) or exposed  
560 positions (582 to 585). Finally, we observe that the effects of synonymous mutations and their  
561 predictors are environment-dependent, with stronger effects at high temperatures.

## 562 4 Conclusion

563 The impact of the codon table on the evolutionary dynamics on fitness landscapes has received  
564 little attention. This is a consequence of the vast size of the nucleotide space and the result-  
565 ing fitness landscape dimensionality, which has led to most studies restricting themselves to  
566 the amino-acid level. This study demonstrates the importance of considering the codon level,  
567 because every single amino-acid position results in a fitness landscape that varies across envi-  
568 ronments. Using rate estimates obtained with *empiricIST*, a new software for the estimation  
569 of growth rates from deep mutational scanning data, we investigated the consequences of in-  
570 cluding synonymous mutations when characterizing the fitness landscape of single amino-acid  
571 positions across environments. Results demonstrate the extent to which synonymous mutations  
572 may impact the topography of the fitness landscape and affect adaptation, as well as their  
573 environmentally-dependent effects. The strongest effects are observed at high temperature,  
574 where the Hsp90 protein is likely under the strongest evolutionary constraint. Interestingly, we  
575 find support for a heavy-tailed distribution of beneficial synonymous effects across all environ-  
576 ments, suggestive of mutations with many small effects, and few with potentially large effects.  
577 A structural analysis indicates that synonymous effects can be mediated by changes in mRNA  
578 stability and variation in codon preference. However, effects are strongly dependent on the  
579 residue position under study, which makes a clear identification of the predictors of synonymous  
580 effects difficult. Overall, this study demonstrates how synonymous mutations can directly im-  
581 pact both the path and endpoint of an adaptive walk, and thus highlights the importance of  
582 their consideration in the study of fitness landscapes.

## 583 5 Acknowledgments

584 We thank the members of the Bank lab for discussion of the manuscript. We thank Dan Bolon  
585 for our long-term collaboration as part of which the data were obtained originally. This work  
586 was supported by Fundação Calouste Gulbenkian and an ERC Starting Grant to JDJ.

## 587 References

588 Agashe D, Martinez-Gomez NC, Drummond DA, Marx CJ (2013). Good codons, bad transcript:  
589 Large reductions in gene expression and fitness arising from synonymous mutations in a key

590 enzyme. *Molecular Biology and Evolution* **30**: 549–560.

591 Agashe D, Sane M, Phalnikar K, Diwan GD, Habibullah A, Martinez-Gomez NC, *et al.* (2016).  
592 Large-Effect Beneficial Synonymous Mutations Mediate Rapid and Parallel Adaptation in a  
593 Bacterium. *Molecular Biology and Evolution* **33**: 1542–1553.

594 Aita T, Iwakura M, Husimi Y (2001). A cross-section of the fitness landscape of dihydrofolate  
595 reductase. *Protein Engineering, Design and Selection* **14**: 633–638.

596 Akashi H (1994). Synonymous codon usage in *Drosophila melanogaster*: Natural selection and  
597 translational accuracy. *Genetics* **136**: 927–935.

598 Bailey SF, Hinz A, Kassen R (2014). Adaptive synonymous mutations in an experimentally  
599 evolved *Pseudomonas fluorescens* population. *Nature Communications* **5**: 1–7.

600 Bali V, Bebok Z (2015). Decoding mechanisms by which silent codon changes influence protein  
601 biogenesis and function. *International Journal of Biochemistry and Cell Biology* **64**: 58–74.

602 Bank C, Hietpas RT, Wong A, Bolon DN, Jensen JD (2014). A Bayesian MCMC approach to  
603 assess the complete distribution of fitness effects of new mutations: Uncovering the potential  
604 for adaptive walks in challenging environments. *Genetics* **196**: 841–852.

605 Bank C, Matuszewski S, Hietpas RT, Jensen JD (2016). On the (un)predictability of a large  
606 intragenic fitness landscape. *Proceedings of the National Academy of Sciences* **113**: 14085–  
607 14090.

608 Bataillon T, Zhang T, Kassen R (2011). Cost of adaptation and fitness effects of beneficial  
609 mutations in *Pseudomonas fluorescens*. *Genetics* **189**: 939–49.

610 Beisel CJ, Rokyta DR, Wichman HA, Joyce P (2007). Testing the extreme value domain of  
611 attraction for distributions of beneficial fitness effects. *Genetics* **176**: 2441–2449.

612 Boone EL, Merrick JR, Krachey MJ (2014). A Hellinger distance approach to MCMC diagnos-  
613 tics. *Journal of Statistical Computation and Simulation* **84**: 833–849.

614 Boucher JI, Cote P, Flynn J, Jiang L, Laban A, Mishra P, *et al.* (2014). Viewing protein fitness  
615 landscapes through a next-gen lens. *Genetics* **198**: 461–471.

616 Brule CE, Grayhack EJ (2017). Synonymous Codons: Choose Wisely for Expression. *Trends in*  
617 *Genetics* **33**: 283–297.

618 Carneiro M, Hartl DL (2010). Adaptive landscapes and protein evolution. *Proceedings of the*  
619 *National Academy of Sciences* **107**: 1747–1751.

620 Chevin LM (2011). On measuring selection in experimental evolution. *Biology letters* **7**: 210–3.

621 Choi JY, Aquadro CF (2016). Recent and Long-Term Selection Across Synonymous Sites in  
622 *Drosophila ananassae*. *Journal of Molecular Evolution* **83**: 50–60.

623 De Visser JAGM, Krug J (2014). Empirical fitness landscapes and the predictability of evolution.  
624 *Nature Reviews Genetics* **15**: 480–490.

625 Drummond DA, Wilke CO (2008). Mistranslation-Induced Protein Misfolding as a Dominant  
626 Constraint on Coding-Sequence Evolution. *Cell* **134**: 341–352.

627 DuMont VB, Fay JC, Calabrese PP, Aquadro CF (2004). DNA variability and divergence at the  
628 Notch locus in *Drosophila melanogaster* and *D. simulans*: A case of accelerated synonymous  
629 site divergence. *Genetics* **167**: 171–185.

630 Eyre-Walker A (2006). The genomic rate of adaptive evolution. *Trends in Ecology and Evolution*  
631 **21**: 569–575.

632 Ferretti L, Schmiegel B, Weinreich D, Yamauchi A, Kobayashi Y, Tajima F, *et al.* (2016). Mea-  
633 suring epistasis in fitness landscapes: The correlation of fitness effects of mutations. *Journal*  
634 *of Theoretical Biology* **396**: 132–143.

635 Firnberg E, Labonte JW, Gray JJ, Ostermeier M (2014). A comprehensive, high-resolution map  
636 of a Gene’s fitness landscape. *Molecular Biology and Evolution* **31**: 1581–1592.

637 Fowler DM, Fields S (2014). Deep mutational scanning: A new style of protein science. *Nature*  
638 *Methods* **11**: 801–807.

639 Frank SA (2014). Generative models versus underlying symmetries to explain biological pattern.  
640 *Journal of Evolutionary Biology* **27**: 1172–1178.

641 Fredrick K, Ibba M (2010). How the sequence of a gene can tune its translation. *Cell* **141**:  
642 227–229.

643 Gelman A, Roberts G, Gilks W (1996). Efficient metropolis jumping rules. In: *Bayesian*  
644 *statistics*, vol. 5, pp. 599–607.

645 Gillespie JH (1983). A simple stochastic gene substitution model. *Theoretical Population Biology*  
646 **23**: 202–215.

647 Gillespie JH (1984). Molecular Evolution Over the Mutational Landscape. *Evolution* **38**: 1116–  
648 1129.

649 Gorter FA, Aarts MGM, Zwaan BJ, de Visser JAGM (2018). Local Fitness Landscapes Predict  
650 Yeast Evolutionary Dynamics in Directionally Changing Environments. *Genetics* **1**: 307–322.

651 Harigaya Y, Parker R (2016). Analysis of the association between codon optimality and mRNA  
652 stability in *Schizosaccharomyces pombe*. *BMC Genomics* **17**: 1–16.

653 Hershberg R, Petrov DA (2009). General rules for optimal codon choice. *PLoS Genetics* **5**:  
654 1–10.

655 Hietpas R, Roscoe B, Jiang L, Bolon DN (2012). Fitness analyses of all possible point mutations  
656 for regions of genes in yeast. *Nature Protocols* **7**: 1382–1396.

657 Hietpas RT, Bank C, Jensen JD, Bolon DNA (2013). Shifting fitness landscapes in response to  
658 altered environments. *Evolution* **67**: 3512–3522.

659 Hietpas RT, Jensen JD, Bolon DNA (2011). Experimental illumination of a fitness landscape.  
660 *Proceedings of the National Academy of Sciences* **108**: 7896–7901.

661 Hilgers V (2006). Translation-independent inhibition of mRNA deadenylation during stress in  
662 *Saccharomyces cerevisiae*. *RNA* **12**: 1835–1845.

663 Hunt RC, Simhadri VL, Iandoli M, Sauna ZE, Kimchi-Sarfaty C (2014). Exposing synonymous  
664 mutations. *Trends in Genetics* **30**: 308–321.

665 Jain K, Krug J, Park SC (2011). Evolutionary advantage of small populations on complex fitness  
666 landscapes. *Evolution* **65**: 1945–1955.

667 Jain K, Seetharaman S (2011). Multiple adaptive substitutions during evolution in novel envi-  
668 ronments. *Genetics* **189**: 1029–1043.

669 Joyce P, Rokyta DR, Beisel CJ, Orr HA (2008). A general extreme value theory model for  
670 the adaptation of DNA sequences under strong selection and weak mutation. *Genetics* **180**:  
671 1627–1643.

672 Knöppel A, Näsval J, Andersson DI (2016). Compensating the Fitness Costs of Synonymous  
673 Mutations. *Molecular Biology and Evolution* **33**: 1461–1477.

674 Kudla G, Murray AW, Tollervey D, Plotkin JB (2009). Coding-Sequence Determinants of Gene  
675 Expression in *Escherichia coli*. *Science* **324**: 255–258.

676 Lanfear R, Kokko H, Eyre-Walker A (2014). Population size and the rate of evolution. *Trends*  
677 *in Ecology and Evolution* **29**: 33–41.

678 Levine TR, Hullett CR (2002). Eta Squared, Partial Eta Squared, and Misreporting of Effect  
679 Size in Communication Research. *Human Communication Research* **28**: 612–625.

680 Lind PA, Berg OG, Andersson DI (2010). Mutational robustness of ribosomal protein genes.  
681 *Science* **330**: 825–827.

682 Lobkovsky AE, Wolf YI, Koonin EV (2011). Predictability of evolutionary trajectories in fitness  
683 landscapes. *PLoS Computational Biology* **7**: 1–11.

684 Lüdecke D (2017). *sjstats: Statistical Functions for Regression Models*. R package version 0.14.0.  
685 **URL:** <https://CRAN.R-project.org/package=sjstats>

686 Markham NR, Zuker M (2008). UNAFold: Software for nucleic acid folding and hybridization.  
687 *Methods in Molecular Biology* **453**: 3–31.

688 Matuszewski S, Hildebrandt ME, Ghenu AH, Jensen JD, Bank C (2016). A statistical guide to  
689 the design of deep mutational scanning experiments. *Genetics* **204**: 77–87.

690 Mishra P, Flynn JM, Starr TN, Bolon DN (2016). Systematic Mutant Analyses Elucidate  
691 General and Client-Specific Aspects of Hsp90 Function. *Cell Reports* **15**: 588–598.

692 Neidhart J, Krug J (2011). Adaptive walks and extreme value theory. *Physical Review Letters*  
693 **107**: 1–4.

694 O’Brien EP, Ciryam P, Vendruscolo M, Dobson CM (2014). Understanding the influence of  
695 codon translation rates on cotranslational protein folding. *Accounts of Chemical Research* **47**:  
696 1536–1544.

697 Orr HA (2000). The rate of adaptation in asexuals. *Genetics* **155**: 961–968.

698 Orr HA (2005). The genetic theory of adaptation: A brief history. *Nature Reviews Genetics* **6**:  
699 119–127.

700 Orr HA (2010). The population genetics of beneficial mutations. *Philosophical Transactions of*  
701 *the Royal Society B: Biological Sciences* **365**: 1195–1201.

702 Parmley JL, Hurst LD (2007). How do synonymous mutations affect fitness? *BioEssays* **29**:  
703 515–519.

704 Perfeito L, Ghozzi S, Berg J, Schnetz K, Lässig M (2011). Nonlinear Fitness Landscape of a  
705 Molecular Pathway. *PLoS Genetics* **7**: e1002160.

706 Plotkin JB, Kudla G (2011). Synonymous but not the same: The causes and consequences of  
707 codon bias. *Nature Reviews Genetics* **12**: 32–42.

708 Poelwijk FJ, Tănase-Nicola S, Kiviet DJ, Tans SJ (2011). Reciprocal sign epistasis is a necessary  
709 condition for multi-peaked fitness landscapes. *Journal of Theoretical Biology* **272**: 141–144.

710 Presnyak V, Alhusaini N, Chen YH, Martin S, Morris N, Kline N, *et al.* (2015). Codon optimality  
711 is a major determinant of mRNA stability. *Cell* **160**: 1111–1124.

712 R Core Team (2017). *R: A Language and Environment for Statistical Computing*. R Foundation  
713 for Statistical Computing, Vienna, Austria. **URL:** <https://www.R-project.org/>

714 Ran W, Higgs PG (2010). The influence of anticodon-codon interactions and modified bases on  
715 codon usage bias in bacteria. *Molecular Biology and Evolution* **27**: 2129–2140.

716 Rodriguez-Verdugo A, Carrillo-Cisneros D, Gonzalez-Gonzalez A, Gaut BS, Bennett AF (2014).  
717 Different tradeoffs result from alternate genetic adaptations to a common environment. *Pro-*  
718 *ceedings of the National Academy of Sciences* **111**: 12121–12126.

719 Rokyta DR, Beisel CJ, Joyce P, Ferris MT, Burch CL, Wichman HA (2008). Beneficial Fitness  
720 Effects Are Not Exponential for Two Viruses. *Journal of molecular evolution* **67**: 368–376.

721 Romero PA, Arnold FH (2009). Exploring protein fitness landscapes by directed evolution.  
722 *Nature Reviews Molecular Cell Biology* **10**: 866–876.

723 Sauna ZE, Kimchi-Sarfaty C (2011). Understanding the contribution of synonymous mutations  
724 to human disease. *Nature Reviews Genetics* **12**: 683–691.

725 Saunders R, Deane CM (2010). Synonymous codon usage influences the local protein structure  
726 observed. *Nucleic Acids Research* **38**: 6719–6728.

727 Schenk MF, Szendro IG, Salverda MLM, Krug J, De Visser JAGM (2013). Patterns of epistasis  
728 between beneficial mutations in an antibiotic resistance gene. *Molecular Biology and Evolution*  
729 **30**: 1779–1787.

730 Schoustra SE, Bataillon T, Gifford DR, Kassen R (2009). The properties of adaptive walks in  
731 evolving populations of fungus. *PLoS Biology* **7**: 1–10.

732 Shabalina SA, Spiridonov NA, Kashina A (2013). Sounds of silence: Synonymous nucleotides  
733 as a key to biological regulation and complexity. *Nucleic Acids Research* **41**: 2073–2094.

734 Shah P, Gilchrist MA (2011). Explaining complex codon usage patterns with selection for  
735 translational efficiency, mutation bias, and genetic drift. *Proceedings of the National Academy  
736 of Sciences* **108**: 10231–10236.

737 Sharp PM, Emery LR, Zeng K (2010). Forces that influence the evolution of codon bias. *Philo-  
738 sophical Transactions of the Royal Society B: Biological Sciences* **365**: 1203–1212.

739 Singh ND, Bauer DuMont VL, Hubisz MJ, Nielsen R, Aquadro CF (2007). Patterns of mutation  
740 and selection at synonymous sites in *Drosophila*. *Molecular Biology and Evolution* **24**: 2687–  
741 2697.

742 Sun Y, Tamarit D, Andersson SG (2016). Switches in Genomic GC Content Drive Shifts of Op-  
743 timal Codons under Sustained Selection on Synonymous Sites. *Genome Biology and Evolution*  
744 p. evw201.

745 Szendro IG, Schenk MF, Franke J, Krug J, De Visser JAGM (2013). Quantitative analyses  
746 of empirical fitness landscapes. *Journal of Statistical Mechanics Theory and Experiment* p.  
747 P01005.

748 Tuller T, Waldman YY, Kupiec M, Ruppin E (2010). Translation efficiency is determined by  
749 both codon bias and folding energy. *Proceedings of the National Academy of Sciences* **107**:  
750 3645–3650.

751 Weinreich DM, Delaney NF, DePristo MA, Hartl DL (2006). Darwinian evolution can follow  
752 only very few mutational paths to fitter proteins. *Science* **312**: 111–114.

753 Wenger JW, Piotrowski J, Nagarajan S, Chiotti K, Sherlock G, Rosenzweig F (2011). Hunger  
754 artists: Yeast adapted to carbon limitation show trade-offs under carbon sufficiency. *PLoS  
755 Genetics* **7**: 1–17.

756 Wolfram Research, Inc (2017). Mathematica v. 11.2. Champaign, Illinois, USA.

757 Wright S (1931). Evolution in mendelian populations. *Genetics* **16**: 97–159.

758 Wu NC, Dai L, Olson CA, Lloyd-Smith JO, Sun R (2016). Adaptation in protein fitness land-  
759 scapes is facilitated by indirect paths. *eLife* **5**: 1–21.

- 760 Yang XX, Maurer KCT, Molanus M, Mager WH, Siderius M, Van Der Vies SM (2006). The  
761 molecular chaperone Hsp90 is required for high osmotic stress response in *Saccharomyces*  
762 *cerevisiae*. *FEMS Yeast Research* **6**: 195–204.
- 763 Yu CH, Dang Y, Zhou Z, Wu C, Zhao F, Sachs MS, *et al.* (2015). Codon Usage Influences the  
764 Local Rate of Translation Elongation to Regulate Co-translational Protein Folding. *Molecular*  
765 *Cell* **59**: 744–754.
- 766 Zagorski M, Burda Z, Waclaw B (2016). Beyond the Hypercube: Evolutionary Accessibility of  
767 Fitness Landscapes with Realistic Mutational Networks. *PLoS Computational Biology* **12**:  
768 1–18.
- 769 Zhang G, Hubalewska M, Ignatova Z (2009). Transient ribosomal attenuation coordinates protein  
770 synthesis and co-translational folding. *Nature Structural and Molecular Biology* **16**: 274–280.
- 771 Zhou T, Weems M, Wilke CO (2009). Translationally optimal codons associate with structurally  
772 sensitive sites in proteins. *Molecular Biology and Evolution* **26**: 1571–1580.
- 773 Zuker M, Mathews D, Turner D (1999). Algorithms and Thermodynamics for RNA secondary  
774 structure prediction: a practical guide. *RNA biochemistry and biotechnology* pp. 1–33.